

Communication

# Centimeter-Scale Curing Depths in Laser-Assisted 3D Printing of Photopolymers Enabled by Er<sup>3+</sup> Upconversion and Green Light-Absorbing Photosensitizer

Adilet Zhakeyev  and Jose Marques-Hueso \* 

Institute of Sensors, Signals and Systems, Heriot-Watt University, Edinburgh EH14 4AS, UK; a.zhakeyev@hw.ac.uk

\* Correspondence: j.marques@hw.ac.uk; Tel.: +44-0-131-451-8268

**Abstract:** Photopolymer resins used in stereolithographic 3D printing are limited to penetration depths of less than 1 mm. Our approach explores the use of near-infrared (NIR) to visible upconversion (UC) emissions from lanthanide-based phosphors to initiate photopolymer crosslinking at a much higher depth. This concept relies on the use of invisibility windows and non-linear optical effects to achieve selective crosslinking in photopolymers. SLA resin formulation capable of absorbing light in the visible region (420–550 nm) was developed, in order to take advantage of efficient green-UC of Er<sup>3+</sup>/Yb<sup>3+</sup> doped phosphor. NIR-green light UC shows versatility in enhancing curing depths in laser patterning. For instance, a structure with a curing depth of 11 ± 0.2 mm, cured width of 496 ± 5 μm and aspect ratios of over 22.2:1 in a single pass via NIR-green light UC. The penetration depth of the reported formulation approached 39 mm. Therefore, this technique would allow curing depths of up to 4 cm. Moreover, it was also demonstrated that this technique can initiate cross-linking directly at the focal point. This shows the potential of NIR-assisted UC as a low-cost method for direct laser writing in volume and 3D printing.

**Keywords:** upconversion; laser patterning; photopolymerization; stereolithography; 3D printing



Citation: Zhakeyev, A.;

Marques-Hueso, J. Centimeter-Scale Curing Depths in Laser-Assisted 3D Printing of Photopolymers Enabled by Er<sup>3+</sup> Upconversion and Green Light-Absorbing Photosensitizer. *Photonics* **2022**, *9*, 498. <https://doi.org/10.3390/photonics9070498>

Received: 23 June 2022

Accepted: 12 July 2022

Published: 16 July 2022

**Publisher's Note:** MDPI stays neutral with regard to jurisdictional claims in published maps and institutional affiliations.



**Copyright:** © 2022 by the authors. Licensee MDPI, Basel, Switzerland. This article is an open access article distributed under the terms and conditions of the Creative Commons Attribution (CC BY) license (<https://creativecommons.org/licenses/by/4.0/>).

## 1. Introduction

Unlike subtractive manufacturing processes, additive manufacturing (AM), also known as three-dimensional (3D) printing, can directly produce complex 3D objects with near-complete design freedom and shows promise in markets that have high demand for customization, flexibility, design complexity and low transportation costs [1]. 3D printing techniques based on photopolymerization such as stereolithography (SLA), digital light processing (DLP) and two-photon polymerization (2PP) exhibit high resolution compared to other 3D printing techniques, particularly 2PP, which is capable of fabricating structures with sub 100 nm features [2]. In SLA/DLP techniques, the curing depths are limited to hundreds of μm because of the low penetration depths of ultraviolet (UV) and blue light due to the presence of UV/blue light absorbing photoinitiators. It was demonstrated by 2PP, which utilizes two-photon absorption (TPA), where a molecule absorbs two photons at the same time by using a virtual state, that the use of a long wavelength excitation source (~800 nm) allows for deeper penetration into the resin than UV light [3,4]. However, 2PP machines are expensive due to the high-intensity femtosecond lasers, which are required since the absorption cross-section of initiators for the two-photon process is very small. Moreover, the time-consuming spot-by-spot printing process and small working distances (<380 μm) of the focusing optics limit the overall size of fabricated objects, which makes 2PP more suitable for fabrication of nano/microstructures.

Upconversion (UC) involves the sequential absorption of low-energy photons (e.g., NIR) before the subsequent emission of a relatively higher energy photon (e.g., UV/visible). Lanthanide-based UC phosphors have real energy levels, so the probability of transition

for a two-photon process can be approximately one million times higher than systems that use virtual energy levels (TPA, second-harmonic generation, etc.), hence the power of the excitation laser can be much smaller and inexpensive diode lasers can be used [5]. It was recently demonstrated that NIR to UV/blue UC based on thulium ( $\text{Tm}^{3+}$ ) and ytterbium ( $\text{Yb}^{3+}$ ) co-doped sodium yttrium fluoride ( $\text{NaYF}_4$ ) can be used for ultra-deep photopolymerization, reaching curing depths of more than 13 cm [6].  $\text{Tm}^{3+}$  doped crystals were also demonstrated to show potential in 3D printing applications [7,8]. In UC, the emission intensity is proportional to the  $n$ th power of the excitation intensity, with  $n$  representing the number of excitation photons required per emitted photon [9]. In the aforementioned  $\text{Tm}^{3+}/\text{Yb}^{3+}$  doped systems used to enhance photopolymerizations, the  $^1\text{G}_4 \rightarrow ^3\text{H}_6$  (475 nm) transition is a three-photon process ( $n = 3$ ), whilst  $^1\text{D}_2 \rightarrow ^3\text{H}_6$  (360 nm) and  $^1\text{D}_2 \rightarrow ^3\text{F}_4$  (450 nm) transitions require four-photon processes ( $n = 4$ ) [10,11]. Moreover, traditional UV or blue light absorbing photoinitiators used in the previous similar studies are not biocompatible, due to toxicity [12].

Erbium ( $\text{Er}^{3+}$ )/Yb $^{3+}$  co-doped  $\text{NaYF}_4$  is one of the most efficient UC materials [13–15]. The green emissions from  $^2\text{H}_{11/2} \rightarrow ^4\text{I}_{15/2}$  (525 nm) and  $^4\text{S}_{3/2} \rightarrow ^4\text{I}_{15/2}$  (547 nm) transitions in  $\text{Er}^{3+}/\text{Yb}^{3+}$  co-doped systems, as shown in Figure 1a, typically involve two-photon UC ( $n = 2$ ) [5,16,17]. This article is an extended version of a brief conference abstract published in reference [18]. Herein, we utilize efficient NIR (980 nm) to green light UC (Figure 2a,b) of  $\text{NaYF}_4:\text{Yb}^{3+},\text{Er}^{3+}$  phosphor for laser patterning of structures with high curing depths, as well as demonstrating the possibility of photocuring directly in volume similar to 2PP. To the best of our knowledge, this is the first demonstration of UC-assisted laser patterning of photopolymers achieved with the green  $\text{Er}^{3+}$  UC emissions, instead of the systems based on UV and/or blue  $\text{Tm}^{3+}$  UC emissions used in the previous studies. The enabling factor for using the green UC, is the synergistic addition of Eosin Y, a visible-light absorbing dye (420–550 nm) and triethanolamine (TEA), as a co-initiator, that bridges the gap towards photopolymerization, as illustrated in Figure 1b [19,20]. Moreover, Eosin Y is a Food and Drug Administration (FDA)-approved photoinitiator, and can be activated with a green light, circumventing the harmful effects from traditionally used UV light, such as DNA damage, accelerated aging of tissues and cancer [20]. This expands the potential of UC-assisted photopolymerization in fabrication of biocompatible objects and devices in situ. The versatility of  $\text{Er}^{3+}$  based formulation was demonstrated in laser patterning of structures with high aspect ratios, as well as ability to only print at the focal point of the laser.

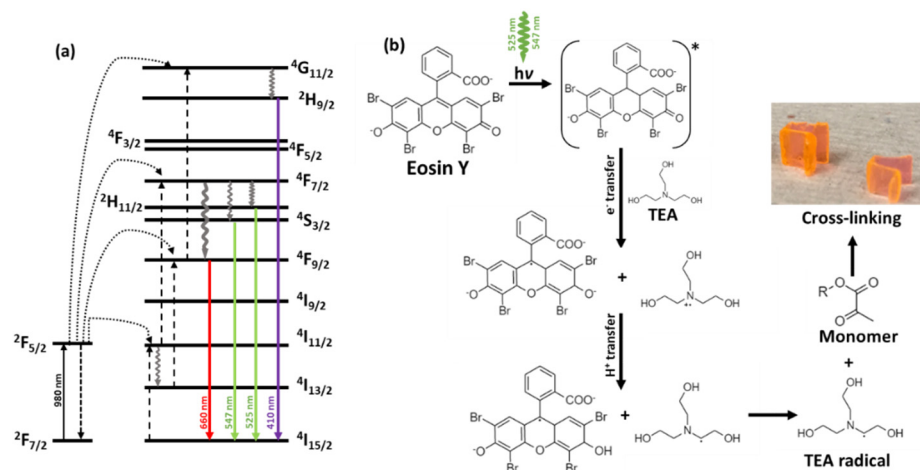


**Figure 1.** (a) Energy level diagram of UC processes in phosphors co-doped with  $\text{Er}^{3+}$  and  $\text{Yb}^{3+}$ ; (b) schematic diagram of type II photoinitiator system based on Eosin Y, used for cross-linking via green UC emissions (\* denotes the excited state of Eosin Y).

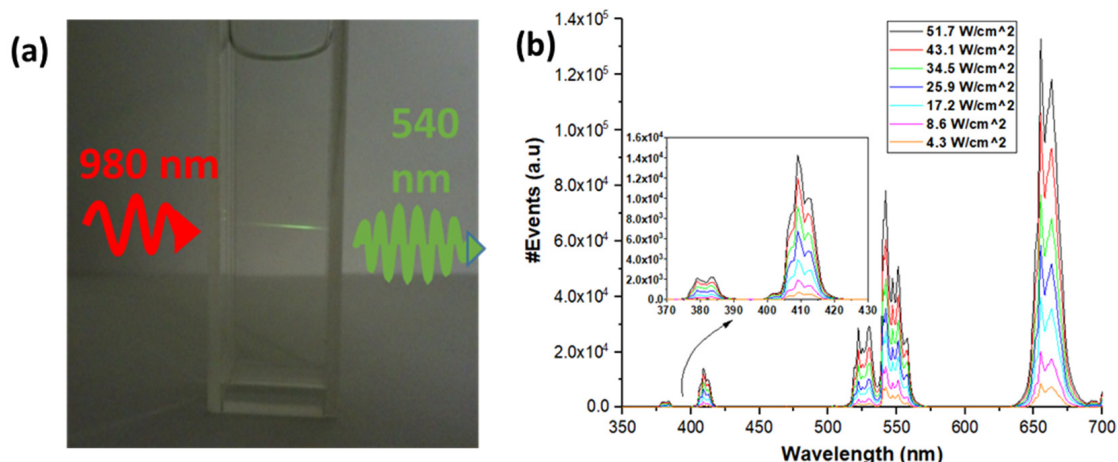


**Figure 2.** (a) Illustration of NIR-green light upconversion; (b) emission profile of bulk NaYF<sub>4</sub>:(20%)Yb<sup>3+</sup>, (3%)Er<sup>3+</sup> phosphor at different 980 nm laser excitation powers densities.

### 2. Materials and Methods

The NaYF<sub>4</sub>: (20%)Yb<sup>3+</sup>, (3%)Er<sup>3+</sup> phosphor, Eosin Y and TEA were obtained from Sigma-Aldrich (St. Louis, MO, USA), and Clear resin (FLGPCL04) was obtained from Formlabs (Somerville, MA, USA). UV/Vis spectra were recorded in a Perkin Elmer Lambda 25 spectrometer. The information on functional groups in resin and laser patterned samples was analyzed in the Nicolet Summit FTIR with a built-in mid- and far-IR attenuated total reflection (ATR) diamond (iD7, Thermo Scientific, Waltham, MA, USA). The double bond conversion was calculated using a method described in literature [21]. The refractive index of Formlabs Clear resin was obtained in an Abbe refractometer (2WAJ, Newtry, Shenzhen, China). Laser patterning was performed using a 980 nm laser diode (OFL371, OdicForce Lasers, Surbiton, UK) and a two-axis stage with a stepper motor controller (A-MCB2, Zaber Technologies, Vancouver, BC, Canada). A calibrated spectrofluorometer (FLS920, Edinburgh Instruments, Livingston, UK) was used for spectral measurements, equipped with a 102 mm inner diameter integrating sphere (HORIBA Jobin-Yvon, Edison, NJ, USA) and a 980 nm laser diode (LSR980NL-3W, Lasever Inc., Ningbo, China) used for excitation. As shown in Equation (1) [14], the external photoluminescence quantum yield (PLQY) was determined by dividing the number of emitted photons (N<sub>em</sub>) by the number of absorbed photons (N<sub>abs</sub>):

$$PLQY = \frac{\text{\#photons emitted}}{\text{\#photons absorbed}} = \frac{N_{em}(\lambda_{ex})}{N_{abs}(\lambda_{ex})} \tag{1}$$

Further details for PLQY measurements can be found in reference [10].

### 3. Results and Discussion

As Figure 2 shows, bulk NaYF<sub>4</sub>: (20%)Yb<sup>3+</sup>, (3%)Er<sup>3+</sup> powder exhibits prominent green (540 nm) and red (660 nm) emissions, as well as small emissions in the blue (410 nm) and UV (380 nm) regions, upon excitation with a 980 nm laser. As expected, the emission intensity increases with a rising excitation power density (Figure 2b).

Figure 3a shows that at power densities above 4 W cm<sup>-2</sup> the emission intensity of red (600–700 nm), green (500–600 nm) and UV/blue (350–425 nm) emissions exhibit a linear relationship with an increase in power density. At laser excitation power density of 17 W cm<sup>-2</sup> PLQY reaches values of 2.3% for red (600–700 nm), 1.4% for green (500–600 nm) and 0.1% for UV/blue (350–425 nm) emissions, respectively. PLQY reaches saturation and starts to decrease slightly when the excitation power density exceeds 25 W cm<sup>-2</sup> as depicted in Figure 3c. It was reported for similar micrometer-sized NaYF<sub>4</sub>:Yb<sup>3+</sup>, Er<sup>3+</sup> phosphors that PLQY exhibits saturation in high power density regime [15,22]. For instance, Kaiser et al. reported that PLQY (integrated over all emission bands) reaches a maximum value of 10.5% at a power density of 30 W cm<sup>-2</sup>, after which saturation was observed [22]. Moreover, it

was also reported that at excitation power densities exceeding  $10 \text{ W cm}^{-2}$ , thermal effects become influential in bulk UC phosphors [23].

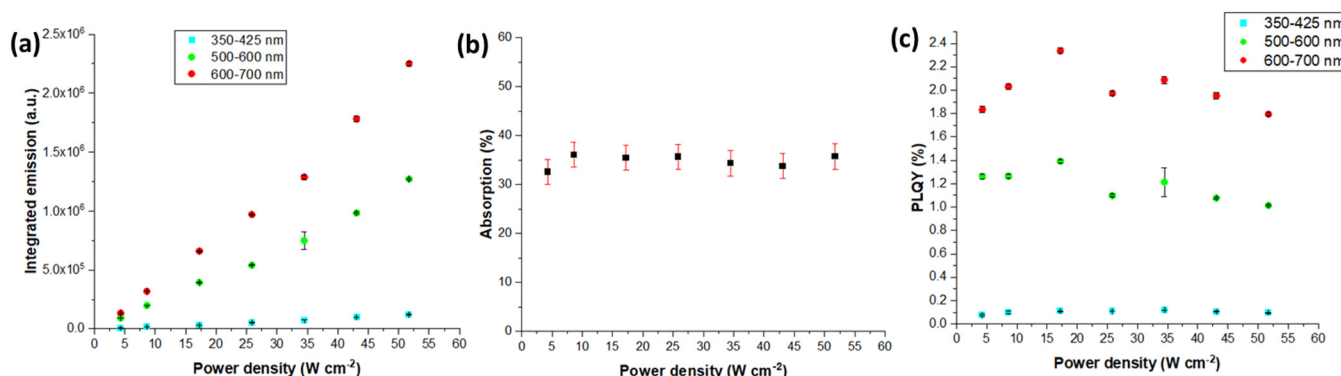


**Figure 3.** The following data was obtained for  $\text{NaYF}_4:(20\%)\text{Yb}^{3+}, (3\%)\text{Er}^{3+}$  phosphor at different 980 nm laser excitation power densities: (a) integrated emission; (b) absorption; (c) PLQY.

The refractive index of Formlabs Clear resin was measured to be 1.479, which matches the refractive index of  $\text{NaYF}_4:(20\%)\text{Yb}^{3+}, (3\%)\text{Er}^{3+}$  phosphor ( $n_p = 1.48$ ) [24]. As a result, this SLA resin was chosen for this study to minimize scattering effects. In order to utilize the emission profile of  $\text{NaYF}_4:(20\%)\text{Yb}^{3+}, (3\%)\text{Er}^{3+}$  for photopolymerization of SLA resin (Formlabs Clear), a suitable photoinitiator must be employed. Most of the commercially available photoinitiators are Norrish Type I initiators, which cleave into free-radical fragments upon light absorption [25–27]. Commonly used benzil ketal photoinitiators (Irgacure 184, Irgacure 369, Irgacure 651 and Irgacure 1173) exhibit fairly low energy  $n \rightarrow \pi^*$  transitions, absorbing light in the UVB and UVA region (up to 350 nm) [26]. In phosphine oxide-based photoinitiators (Irgacure 819, TPO, TPO-L and LAP), the phosphorous atom lowers the energy level of the  $\pi^*$  state. As a result, the peak of  $n \rightarrow \pi^*$  transition is shifted towards 400 nm [25]. Germanium-based photoinitiators such as Ivocerin exhibit a significant redshift of  $n \rightarrow \pi^*$  transition, showing a strong absorption in the blue light region ( $\lambda_{\text{max}} = 408 \text{ nm}$ ) [28,29]. Another example of metallocene initiators include titanocenes, such as fluorinated diaryl titanocene (Irgacure 784) and bis(pentafluorophenyl)titanocene, which exhibits  $\lambda_{\text{max}}$  at 465 nm. Formlabs Clear resin already contains a proprietary Type I initiator, which absorbs light up to 420 nm and matches the 410 nm emission peak of  $\text{NaYF}_4:(20\%)\text{Yb}^{3+}, (3\%)\text{Er}^{3+}$  as illustrated in Figure 4a. However, Type I initiators are not suited for excitation with the green emissions (500–575 nm) of  $\text{NaYF}_4:(20\%)\text{Yb}^{3+}, (3\%)\text{Er}^{3+}$  phosphor.

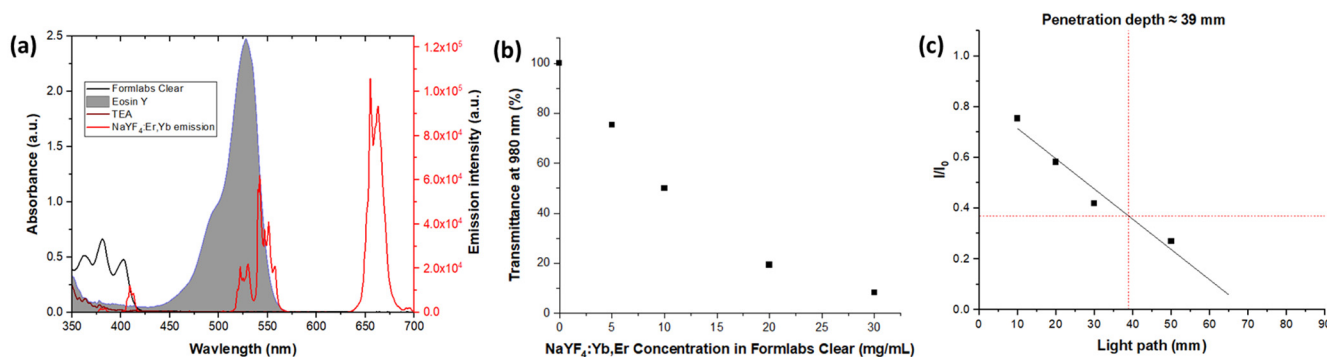


**Figure 4.** (a) Absorption spectrum of the photoinitiation system matched with phosphor emissions; (b) transmittance @ 980 nm of resin formulation with different  $\text{NaYF}_4:(20\%)\text{Yb}^{3+}, (3\%)\text{Er}^{3+}$  loadings; (c) transmittance @ 980 nm of 5 mg mL  $\text{NaYF}_4:(20\%)\text{Yb}^{3+}, (3\%)\text{Er}^{3+}$  loading at different path lengths.

Type II photoinitiating systems usually consist of an uncleavable photosensitizer (CQ, benzophenones, thioxanones, etc.) and a co-initiator (usually tertiary amines) [26].

Upon absorption of the light of an appropriate wavelength, photosensitizers form excited triplet state and undergo hydrogen abstraction or electron transfer in the presence of a co-initiator [25]. Eosin Y is a photosensitizer, which exhibits maximum absorbance at 530 nm and closely matches the green emissions of  $\text{NaYF}_4$ : (20%) $\text{Yb}^{3+}$ , (3%) $\text{Er}^{3+}$  as shown in Figure 4a. When used alongside a co-initiator (synergist), such as TEA, it can be effectively used as a type II photoinitiator in photopolymerization reactions (Figure 1b).

Figure 4b depicts the comparison of Formlabs Clear resin with different  $\text{NaYF}_4$ : (20%) $\text{Yb}^{3+}$ , (3%) $\text{Er}^{3+}$  concentrations with respect to transmission at 980 nm. In order to ensure sufficient transmission of excitation light, the phosphor concentration of  $5 \text{ mg mL}^{-1}$  was chosen, which shows transmittance of 72% for a 10 mm light path at 980 nm (molar extinction coefficient =  $5.1 \text{ M}^{-1} \text{ cm}^{-1}$ ). At this concentration, the penetration depth ( $37\% I/I_0$ ) was measured to be 39 mm as shown in Figure 4c. Figure 5 illustrates that the formulation containing Eosin Y effectively absorbs the upconverted green emissions, with only red emissions visible. Initial observations reveal that the stability of the photosensitive resin is similar to commercial formulations, and there is no accelerated degrading. FTIR spectra of samples before and after laser patterning were collected in order to establish the double bond conversion (DBC) achievable via UC-assisted cross-linking, as shown in Figure 6. This was achieved by observing aliphatic  $\text{C}=\text{C}$  bond ( $1637 \text{ cm}^{-1}$ ) conversion with respect to the carbonyl  $\text{C}=\text{O}$  peak ( $1697 \text{ cm}^{-1}$ ) as the internal standard. The laser patterning of Formlabs Clear resin with the green  $\text{Er}^{3+}$  emissions, resulted in the DBC of 49%. This compares well with the previously reported DBC of around 40% for blank Formlabs Clear resin after 60 s of irradiation with UV light [30].

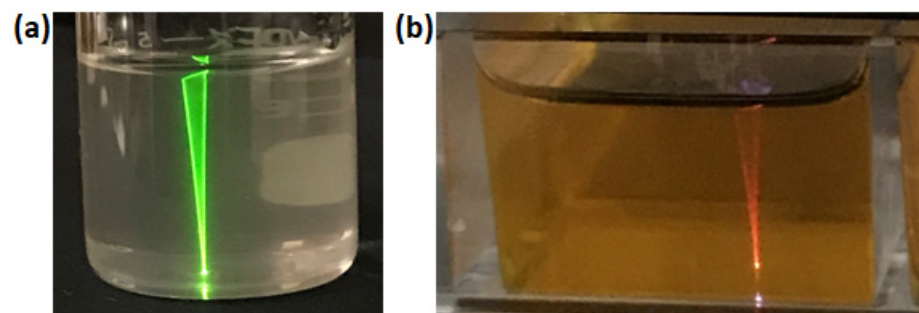


**Figure 5.** Resin formulation: (a) without; (b) with 0.05 wt% Eosin Y and 2.5 wt% TEA upon excitation with a 980 nm laser.

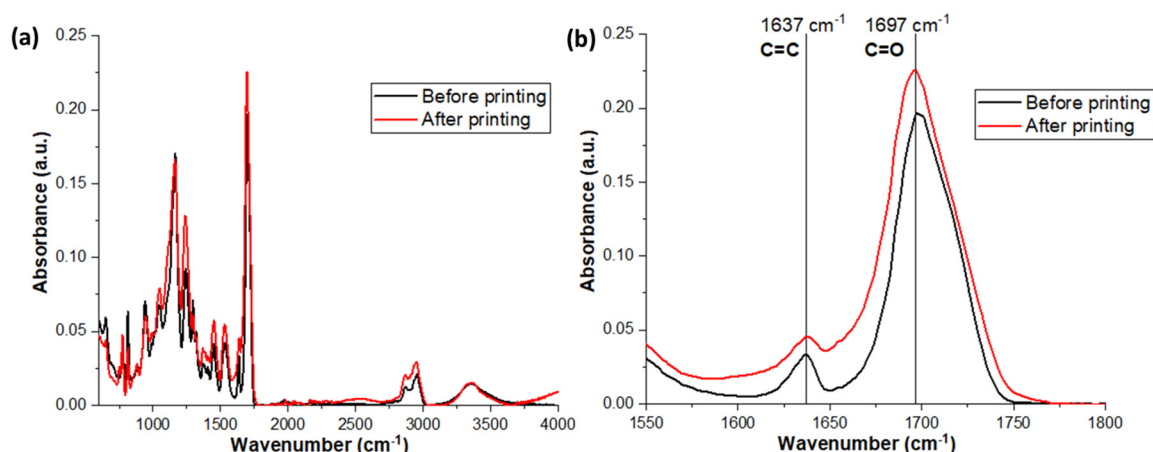


**Figure 6.** Comparison of FTIR spectra of 0.05 wt% Eosin Y and 2.5 wt% TEA samples before and after crosslinking: (a) full range; (b) 1550 to  $1800 \text{ cm}^{-1}$ .

This formulation was used for laser patterning of Formlabs Clear resin with a 980 nm laser diode. At the laser power of  $200 \text{ mW}$  and laser scanning speed of  $0.02 \text{ mm s}^{-1}$ , cross-linking all the way up to the surface of the resin was achieved in a single pass, resulting in

curing depth of  $11 \pm 0.2$  mm, cured width of  $496 \pm 5$   $\mu\text{m}$  and aspect ratios of over 22.2:1 as shown in Figure 7. Since the penetration depth of this formulation is 39 mm, technically curing depths of up to 4 cm can be achieved.

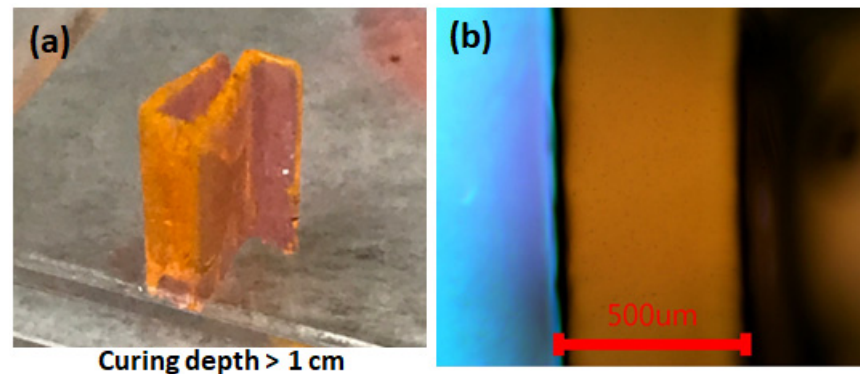


**Figure 7.** NIR-green light UC assisted laser patterning of a 3D structure in a single pass: (a) photograph; (b) optical microscope image of the top-down view of the sample.

Moreover, NIR-green light UC allows for selective cross-linking at the focal point of the laser, with the cured width of  $437 \pm 9$   $\mu\text{m}$  as shown in Figure 8. This was achieved when the laser power was set to 240 mW, laser scanning speed to  $0.2 \text{ mm s}^{-1}$  and number of passes = 4. This demonstrates that this technique shows potential in high-yield and inexpensive “direct laser writing” (DLW) 3D printing, by using a low-cost 980 nm laser diode (<£30), in comparison to the high-intensity femtosecond lasers used in 2PP.

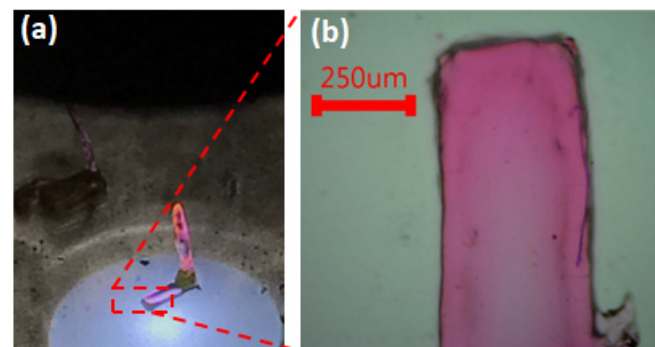


**Figure 8.** NIR-green light UC assisted laser cross-linking at the focal point: (a) photograph; (b) optical microscope image the top-down view of the sample.

#### 4. Conclusions

A new formulation based on Eosin Y and NIR-green light UC has enabled the patterning of structures with curing depths of over 10 mm, compared to less than 1 mm achieved in traditional UV/blue light-based curing and 3D printing techniques. This method allows the transformation of photopolymerization from thin 2D layers to the fabrication of thick 3D layers with high aspect ratios in just one passing. This technique has shown the capability of producing samples with 22.2:1 aspect ratio. Moreover, this technique can also be applied as a low-cost method for DLW 3D printing, opening the door for new approaches, such as multi-material SLA.

**Author Contributions:** Experimental investigation, analysis and writing—original draft preparation, A.Z. Conceptualization, project management, funding and supervision, J.M.-H. All authors have read and agreed to the published version of the manuscript.

**Funding:** This research work is supported by UK Engineering and Physical Science Research Council (EPSRC) Grant EP/T013680/1.

**Institutional Review Board Statement:** Not applicable.

**Informed Consent Statement:** Not applicable.

**Data Availability Statement:** The data that support the findings of this study are available from the corresponding author upon reasonable request.

**Acknowledgments:** The authors thank the financial support from the Engineering and Physical Sciences Research Council of the United Kingdom (EPSRC) Grant EP/T013680/1.

**Conflicts of Interest:** The authors declare no conflict of interest.

## References

1. Weller, C.; Kleer, R.; Piller, F.T. Economic implications of 3D printing: Market structure models in light of additive manufacturing revisited. *Int. J. Prod. Econ.* **2015**, *164*, 43–56. [\[CrossRef\]](#)
2. Park, S.-H.; Yang, D.-Y.; Lee, K.-S. Two-photon stereolithography for realizing ultraprecise three-dimensional nano/microdevices. *Laser Photon. Rev.* **2009**, *3*, 1–11. [\[CrossRef\]](#)
3. Malval, J.-P.; Jin, M.; Morlet-Savary, F.; Chaumeil, H.; Defoin, A.; Soppera, O.; Scheul, T.; Bouriau, M.; Baldeck, P.L. Enhancement of the Two-Photon Initiating Efficiency of a Thioxanthone Derivative through a Chevron-Shaped Architecture. *Chem. Mater.* **2011**, *23*, 3411–3420. [\[CrossRef\]](#)
4. Li, Z.; Pucher, N.; Cicha, K.; Torgersen, J.; Ligon, S.C.; Ajami, A.; Husinsky, W.; Rosspeintner, A.; Vauthey, E.; Naumov, S.; et al. A Straightforward Synthesis and Structure–Activity Relationship of Highly Efficient Initiators for Two-Photon Polymerization. *Macromolecules* **2013**, *46*, 352–361. [\[CrossRef\]](#)
5. Auzel, F. Upconversion and Anti-Stokes Processes with f and d Ions in Solids. *Chem. Rev.* **2004**, *104*, 139–174. [\[CrossRef\]](#) [\[PubMed\]](#)
6. Liu, R.; Chen, H.; Li, Z.; Shi, F.; Liu, X. Extremely deep photopolymerization using upconversion particles as internal lamps. *Polym. Chem.* **2016**, *7*, 2457–2463. [\[CrossRef\]](#)
7. Méndez-Ramos, J.; Ruiz-Morales, J.C.; Acosta-Mora, P.; Khaidukov, N.M. Infrared-light induced curing of photosensitive resins through photon up-conversion for novel cost-effective luminescent 3D-printing technology. *J. Mater. Chem. C* **2016**, *4*, 801–806. [\[CrossRef\]](#)
8. Rocheva, V.V.; Koroleva, A.V.; Savelyev, A.G.; Khaydukov, K.V.; Generalova, A.N.; Nechaev, A.V.; Guller, A.E.; Semchishen, V.A.; Chichkov, B.N.; Khaydukov, E.V. High-resolution 3D photopolymerization assisted by upconversion nanoparticles for rapid prototyping applications. *Sci. Rep.* **2018**, *8*, 3663. [\[CrossRef\]](#)
9. Pollnau, M.; Gamelin, D.R.; Lüthi, S.R.; Güdel, H.U.; Hehlen, M.P. Power dependence of upconversion luminescence in lanthanide and transition-metal-ion systems. *Phys. Rev. B* **2000**, *61*, 3337–3346. [\[CrossRef\]](#)
10. Alyatkin, S.; Asharchuk, I.; Khaydukov, K.; Nechaev, A.; Lebedev, O.; Vainer, Y.; Semchishen, V.; Khaydukov, E. The influence of energy migration on luminescence kinetics parameters in upconversion nanoparticles. *Nanotechnology* **2016**, *28*, 35401. [\[CrossRef\]](#)
11. Wang, G.; Qin, W.; Wang, L.; Wei, G.; Zhu, P.; Kim, R. Intense ultraviolet upconversion luminescence from hexagonal NaYF<sub>4</sub>:Yb<sup>3+</sup>/Tm<sup>3+</sup> microcrystals. *Opt. Express* **2008**, *16*, 11907–11914. [\[CrossRef\]](#) [\[PubMed\]](#)
12. Carve, M.; Wlodkovic, D. 3D-Printed Chips: Compatibility of Additive Manufacturing Photopolymeric Substrata with Biological Applications. *Micromachines* **2018**, *9*, 91. [\[CrossRef\]](#) [\[PubMed\]](#)
13. MacDougall, S.K.W.; Ivaturi, A.; Marques-Hueso, J.; Krämer, K.W.; Richards, B.S. Ultra-high photoluminescent quantum yield of  $\beta$ -NaYF<sub>4</sub>: 10% Er<sup>3+</sup> via broadband excitation of upconversion for photovoltaic devices. *Opt. Express* **2012**, *20*, A879–A887. [\[CrossRef\]](#) [\[PubMed\]](#)
14. Jones, C.M.S.; Gakamsky, A.; Marques-Hueso, J. The upconversion quantum yield (UCQY): A review to standardize the measurement methodology, improve comparability, and define efficiency standards. *Sci. Technol. Adv. Mater.* **2021**, *22*, 810–848. [\[CrossRef\]](#)
15. Jones, C.M.S.; Biner, D.; Misopoulos, S.; Krämer, K.W.; Marques-Hueso, J. Optimized photoluminescence quantum yield in upconversion composites considering the scattering, inner-filter effects, thickness, self-absorption, and temperature. *Sci. Rep.* **2021**, *11*, 13910. [\[CrossRef\]](#)
16. Ding, M.; Chen, D.; Yin, S.; Ji, Z.; Zhong, J.; Ni, Y.; Lu, C.; Xu, Z. Simultaneous morphology manipulation and upconversion luminescence enhancement of  $\beta$ -NaYF<sub>4</sub>:Yb<sup>3+</sup>/Er<sup>3+</sup> microcrystals by simply tuning the KF dosage. *Sci. Rep.* **2015**, *5*, 12745. [\[CrossRef\]](#)
17. Bednarkiewicz, A.; Wawrzynczyk, D.; Gagor, A.; Kepinski, L.; Kurnatowska, M.; Krajczyk, L.; Nyk, M.; Samoc, M.; Strek, W. Giant enhancement of upconversion in ultra-small Er<sup>3+</sup>/Yb<sup>3+</sup>:NaYF<sub>4</sub> nanoparticles via laser annealing. *Nanotechnology* **2012**, *23*, 145705. [\[CrossRef\]](#)
18. Zhakeyev, A.; Marques-Hueso, J. Nonlinear Upconversion Effect for Enhancement of Curing Depths in Laser-Assisted 3D Printing of Photopolymers. In Proceedings of the 5th International Conference on Optics, Photonics and Lasers (OPAL' 22), Tenerife (Canary Islands), Spain, 18–20 May 2022; Yurish, S., Ed.; IFSA Publishing: Barcelona, Spain, 2022; pp. 85–86.
19. Kaastrup, K.; Sikes, H.D. Using photo-initiated polymerization reactions to detect molecular recognition. *Chem. Soc. Rev.* **2016**, *45*, 532–545. [\[CrossRef\]](#)

20. Noshadi, I.; Hong, S.; Sullivan, K.E.; Shirzaei Sani, E.; Portillo-Lara, R.; Tamayol, A.; Shin, S.R.; Gao, A.E.; Stoppel, W.L.; Black III, L.D.; et al. In vitro and in vivo analysis of visible light crosslinkable gelatin methacryloyl (GelMA) hydrogels. *Biomater. Sci.* **2017**, *5*, 2093–2105. [[CrossRef](#)]
21. Rueggeberg, F.A.; Hashinger, D.T.; Fairhurst, C.W. Calibration of FTIR conversion analysis of contemporary dental resin composites. *Dent. Mater.* **1990**, *6*, 241–249. [[CrossRef](#)]
22. Kaiser, M.; Würth, C.; Kraft, M.; Hyppänen, I.; Soukka, T.; Resch-Genger, U. Power-dependent upconversion quantum yield of NaYF<sub>4</sub>:Yb<sup>3+</sup>,Er<sup>3+</sup> nano- and micrometer-sized particles—measurements and simulations. *Nanoscale* **2017**, *9*, 10051–10058. [[CrossRef](#)] [[PubMed](#)]
23. Joseph, R.E.; Jiménez, C.; Hudry, D.; Gao, G.; Busko, D.; Biner, D.; Turshatov, A.; Krämer, K.; Richards, B.S.; Howard, I.A. Critical Power Density: A Metric To Compare the Excitation Power Density Dependence of Photon Upconversion in Different Inorganic Host Materials. *J. Phys. Chem. A* **2019**, *123*, 6799–6811. [[CrossRef](#)] [[PubMed](#)]
24. Jones, C.M.S.; Panov, N.; Skripka, A.; Gibbons, J.; Hesse, F.; Bos, J.-W.G.; Wang, X.; Vetrone, F.; Chen, G.; Hemmer, E.; et al. Effect of light scattering on upconversion photoluminescence quantum yield in microscale-to-nanoscale materials. *Opt. Express* **2020**, *28*, 22803–22818. [[CrossRef](#)] [[PubMed](#)]
25. Bagheri, A.; Jin, J. Photopolymerization in 3D Printing. *ACS Appl. Polym. Mater.* **2019**, *1*, 593–611. [[CrossRef](#)]
26. Ligon, S.C.; Liska, R.; Stampfl, J.; Gurr, M.; Mülhaupt, R. Polymers for 3D Printing and Customized Additive Manufacturing. *Chem. Rev.* **2017**, *117*, 10212–10290. [[CrossRef](#)]
27. Zhang, J.; Xiao, P. 3D printing of photopolymers. *Polym. Chem.* **2018**, *9*, 1530–1540. [[CrossRef](#)]
28. Moszner, N.; Zeuner, F.; Lamparth, I.; Fischer, U.K. Benzoylgermanium Derivatives as Novel Visible-Light Photoinitiators for Dental Composites. *Macromol. Mater. Eng.* **2009**, *294*, 877–886. [[CrossRef](#)]
29. Ganster, B.; Fischer, U.K.; Moszner, N.; Liska, R. New Photocleavable Structures, 4. *Macromol. Rapid Commun.* **2008**, *29*, 57–62. [[CrossRef](#)]
30. Zhakeyev, A.; Jones, M.C.; Thomson, C.G.; Tobin, J.M.; Wang, H.; Vilela, F.; Xuan, J. Additive manufacturing of intricate and inherently photocatalytic flow reactor components. *Addit. Manuf.* **2021**, *38*, 101828. [[CrossRef](#)]